Scattering of Continental Shelf Waves at a Discontinuity in Shelf Width*

JOHN L. WILKIN AND DAVID C. CHAPMAN

Woods Hole Oceanographic Institution, Woods Hole, MA 02543

(Manuscript received 19 March 1986, in final form 8 September 1986)

ABSTRACT

An analytical solution is presented for the scattering of a free shelf wave incident upon a discontinuity in shelf width in a barotropic ocean. The discussion of solutions relying on backscattered free-waves with large wavenumbers which may not exist in a realistically stratified ocean is avoided by considering only the range of parameters over which energy transmission is nearly 100%. There is a substantial transfer of energy to modes other than that of the incident wave. The mode most readily excited is that which has the cross-shelf structure most closely coinciding with that of the incident wave. The resultant presence of multiple modes produces a strong alongshelf modulation in flow intensity and phase progression downstream of the scattering region which may affect the interpretation of shelf wave observations. A nondispersive long shelf wave pulse is shown to scatter into a train of pulses of differing mode numbers, each propagating at its own free wave speed.

1. Introduction

A major part of the large-scale, low-frequency current and sea-level variability along many coastlines appears to be associated with freely propagating, remotely wind-forced, coastally trapped waves (CTWs). This statement is supported both by examination of the spatial coherence between sea-level records and wind fields along the Pacific coasts of North America (Halliwell and Allen, 1984), Mexico (Enfield and Allen, 1983) and Peru (Smith, 1978; Brink, 1982b) and by so-called "first-order wave equation" (FOWE) studies.

In the latter, observed alongshelf winds are assumed to generate long CTWs which propagate along the coast according to the theory of Gill and Schumann (1974) which has since been generalized by Clarke (1977), Brink and Allen (1978), Brink (1982a) and Clarke and Van Gorder (1986). Variations in bottom topography and coastline shape are allowed only parametrically through slow alongshelf changes in the long-wave phase speeds, wind-coupling coefficients and bottom-friction coefficients. Along relatively straight coasts, this FOWE approach has been quite successful. For example, Battisti and Hickey (1984) obtained good visual agreement between observed and predicted subsurface pressure variations along the Oregon and Washington coasts by modeling only the lowest mode CTW. However, most coastlines can vary significantly over spatial scales much shorter than the CTW length scales which may cause appreciable scattering of CTW signals into other modes. The importance of such scattering processes at places where the shelf width changes sharply, such as the Gulf of California or the region around Point Conception, California, is unclear. However, it is of interest to note that observed shelf wave signals south of the Gulf of California were found to be uncorrelated with sea-level fluctuations on either side of Baja California (Enfield and Allen, 1983) and little CTW activity seen at northern sites was found to be generated south of Point Conception (Battisti and Hickey, 1984).

Previous theoretical studies of shelf wave scattering have considered small variations in bottom topography (Chao et al., 1979; Brink, 1980; Brink, 1986), small perturbations to a straight coast (Allen, 1976; Buchwald, 1977) or slow alongshelf variations on a scale much longer than the shelf width (Grimshaw, 1977). In this paper, a theoretical investigation of the scattering of free shelf waves by an abrupt change in shelf width in a barotropic ocean is presented.

The principal limitation on the usefulness of the results presented here is the neglect of stratification. In a barotropic ocean, a free shelf wave is limited to a finite subinertial frequency range above which it cannot propagate. At low wavenumbers, the wave's group velocity is cyclonic with respect to the deep sea and decreases with increasing wavenumber eventually passing through zero, provided the bottom slope is bounded, to a region of short waves with group velocity in the opposite sense (Huthnance, 1975). Introducing stratification increases the wave frequency at all wavenumbers (Huthnance, 1978) and this can qualitatively alter the behavior of each mode at high wavenumbers when the stratification is sufficiently strong to cause the dispersion curves to increase monotonically to the Coriolis frequency f. In this case, each mode can occur at any subinertial frequency but is limited in wavenumber. There are then no zero group velocity points, and consequently, phase and energy always propagate in the

* Woods Hole Oceanographic Contribution No. 6137.

same direction. Thus a reflected or backscattered flux of energy is not possible. Chapman (1983) has demonstrated that such a wavenumber-limited regime generally occurs on shelves where $Nh_0/fL > 1$, where N is the maximum buoyancy frequency, h_0 the deep-sea depth and L the shelf-slope width. Furthermore, computations of free-wave dispersion curves using observed geometry and stratification for many shelves, including the Pacific Northwest (Battisti and Hickey, 1984) and Peru (Brink, 1982b), suggest that wavenumber-limited free waves are more nearly the rule than the exception. Therefore, the results discussed in this paper will concentrate on those situations in which little or no backscattering occurs.

The theoretical formulation of the scattering problem is described in section 2 and the results of the solution are presented in section 3. These are discussed in section 4 and a summary of the salient features is given in section 5.

2. Problem formulation and solution

An inviscid, barotropic, coastal ocean on a Northern Hemisphere f-plane is considered. Making the rigid-lid approximation, the linear shallow water equations become

$$u_t - fv = -g\eta_x \tag{1a}$$

$$v_t + fu = -g\eta_y \tag{1b}$$

$$(hu)_x + (hv)_y = 0 \tag{2}$$

where u and v are the cross-shelf (x) and alongshelf (y) components of velocity, respectively, η is the surface height perturbation, g the gravitational acceleration, f the Coriolis parameter and h the depth. Subscripts denote partial differentiation. Defining a transport streamfunction

$$hu = -\psi_y; \quad hv = \psi_x \tag{3}$$

(1) and (2) combine to yield a vorticity equation

$$\left[\left(\frac{\psi_y}{h}\right)_y + \left(\frac{\psi_x}{h}\right)_x\right]_t - f\left[\left(\frac{\psi_y}{h}\right)_x - \left(\frac{\psi_x}{h}\right)_y\right] = 0. \tag{4}$$

The depth is assumed to increase exponentially offshore

$$h(x) = h_0 e^{-2\lambda x} \tag{5}$$

where h_0 is the depth at the outer edge of the shelf. For large values of λ, the shelf drops off steeply at its outer limit, while for smaller values it is more uniformly and weakly sloping. Therefore, λ will be referred to as the slope steepness. For a traveling wave with frequency ω and alongshelf wavenumber l, ψ takes the form

$$\psi = \phi(x) e^{i(ly-\omega t)}. \tag{6}$$

Substitution of (5) and (6) into (4) shows that the cross-shelf structure function $\phi(x)$ satisfies

$$\phi_{xx} + 2\lambda\phi_x + \left(\frac{2\lambda f l}{\omega} - l^2\right)\phi = 0. \tag{7}$$

A straight coast is placed at $x = L$. The origin $x = 0$ is the offshore edge of the shelf where a wall rather than an open boundary has been placed for analytical convenience. This retains the qualitative properties of the open boundary (Brink, 1980) while making the cross-shelf modal structure independent of alongshelf wavenumber and allowing the use of a simple mode-matching method. The boundary conditions of no flow through the walls require that ψ be constant along $x = 0$ and $x = L$. Without loss of generality the constant may be chosen to be zero so that

$$\phi(0) = \phi(L) = 0. \tag{8}$$

Solving (7) subject to (8) yields

$$\phi_n(x) = e^{-\lambda x} \sin k_n x \tag{9}$$

where

$$k_n = \frac{n\pi}{L}; \quad n = 1, 2, 3 \cdots \tag{10}$$

with n being the mode number. The dispersion relation for mode n is

$$\omega = \frac{2\lambda f l_n}{k_n^2 + \lambda^2 + l_n^2}. \tag{11}$$

The ϕ_n satisfy an orthogonality condition

$$\frac{2}{L}\int_0^L \phi_n e^{2\lambda x}\phi_m dx = \delta_{mn} \tag{12}$$

where δ_{mn} is the Kronecker delta. Were the wall to be replaced by the more realistic condition that the shelf abuts a semi-infinite flat-bottom ocean, (10) would be replaced by

$$\tan k_n L = \frac{-k_n}{\lambda + l_n}. \tag{13}$$

The resultant effect on the free-wave dispersion curves is shown in Fig. 1 for the case $\lambda L = 2.25$. The presence of the offshore wall has no qualitative, and little quantitative effect, so its use should not limit the applicability of the present results.

The scattering problem considered is that of a shelf wave traveling in a channel whose width changes abruptly from L_1 to L_2 at $y = 0$ (see Fig. 2). A wave of amplitude $\hat{A}$, wavenumber $\hat{l}$ and mode number I is assumed to be incident upon the coastline bend from $y = -\infty$. The solution on either side of the bend may then be written

$$\psi_- = \hat{A}\phi_{1I} e^{i(\hat{l}y-\omega t)} + \sum_{p=1}^{\infty} A_p \phi_{1p} e^{i(l_{1p}y-\omega t)}, \quad y<0 \tag{14a}$$

$$\psi_+ = \sum_{q=1}^{\infty} B_q \phi_{2q} e^{i(l_{2q}y-\omega t)}, \quad y>0 \tag{14b}$$

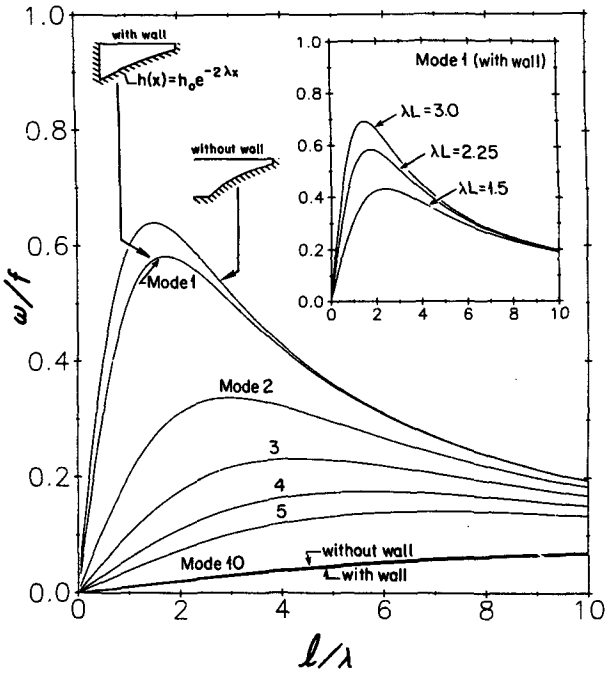

FIG. 1. Barotropic shelf wave dispersion curves for a shelf with exponential depth profile for the case $\lambda L = 2.25$. For modes 1 and 10 a comparison is made of two offshore boundary conditions. The remaining curves are computed with an offshore wall. Inset shows mode 1 dispersion curves for a range of λL values.

where

$$\phi_{1p} = e^{-\lambda x}\sin k_{1p}x; \quad k_{1p} = \frac{p\pi}{L_1}; \quad p = 1, 2, 3 \cdots \tag{15a}$$

$$\phi_{2q} = e^{-\lambda x}\sin k_{2q}x; \quad k_{2q} = \frac{q\pi}{L_2}; \quad q = 1, 2, 3 \cdots \tag{15b}$$

and k_{1p}, l_{1p} and k_{2q}, l_{2q} satisfy (11). The first subscript (1 or 2) on k, l and ϕ denotes the shelf width (L_1 or L_2) to which the variable corresponds. The second subscript is the mode number and corresponds to n in equations (9) through (11). The dispersion relation (11) is a quadratic equation for l_n with the solution

$$l_n = \frac{f\lambda}{\omega} \pm \left[\left(\frac{f\lambda}{\omega}\right)^2 - (k_n^2 + \lambda^2)\right]^{1/2}. \tag{16}$$

If $(f\lambda/\omega)^2 > k_n^2 + \lambda^2$, then l_n is real and mode n propagates energy as a free wave. Since the l_{1p} represent reflected waves and the l_{2q} are transmitted waves, the radiation conditions require that if l_{1p}, l_{2q} are real, they must correspond to negative, positive group velocity, respectively. This means that the + (−) sign in (16) must be used to compute real $l_{1p}(l_{2q})$. If l_{1p}, l_{2q} are complex, i.e., $(f\lambda/\omega)^2 < k_n^2 + \lambda^2$, then the sign of the imaginary part must be selected to give an evanescent alongshelf structure trapped at the discontinuity (i.e., exponentially decaying away from $y = 0$). Thus, the − (+) sign must be used to compute complex $l_{1p}(l_{2q})$.

The complex scattered wave amplitudes A_p, B_q are determined by matching (i) surface height η and (ii) alongshelf transport ψ_x along the common fluid boundary and by requiring $\psi = 0$ along the solid wall at $y = 0$, $L_1 < x < L_2$ because it is a continuation of the coastal streamline. To match ψ_x it is sufficient to match ψ since ψ is continuously differentiable in x and $\psi_- = \psi_+$ at the solid walls ($x = 0$, L).

For $L_2 > L_1$ the matching conditions are

$$\psi_+ = \begin{cases} \psi_-, & 0 < x < L_1 \\ 0, & L_1 < x < L_2 \end{cases} \tag{17a}$$

$$\eta_+ = \eta_-, \quad 0 < x < L_1. \tag{17b}$$

Integration of the alongshelf momentum equation (1b) yields an expression for η

$$\eta_- = \frac{1}{gh}\hat{A}\left(f\phi_{1I} + \frac{\omega}{\hat{l}}\frac{d\phi_{1I}}{dx}\right)e^{i(\hat{l}y-\omega t)} + \frac{1}{gh}\sum_{p=1}^{\infty} A_p\left(f\phi_{1p} + \frac{\omega}{l_{1p}}\frac{d\phi_{1p}}{dx}\right)e^{i(l_{1p}y-\omega t)} \tag{18a}$$

$$\eta_+ = \frac{1}{gh}\sum_{q=1}^{\infty} B_q\left(f\phi_{2q} + \frac{\omega}{l_{2q}}\frac{d\phi_{2q}}{dx}\right)e^{i(l_{2q}y-\omega t)} + \frac{f}{gh_0}Ce^{-i\omega t} \tag{18b}$$

where C is a constant of integration corresponding to the Kelvin wave mode. This is easily seen by obtaining the solution for a divergent barotropic Kelvin wave and formally taking the limit of a rigid-lid boundary condition. Under a rigid lid, the phase speed and horizontal spatial scales of the Kelvin mode become infinite, thereby reducing the wave to a time-varying but spatially uniform fluctuation in the pressure field throughout the channel. The velocities vanish as the reciprocal of phase speed and thus the Kelvin mode

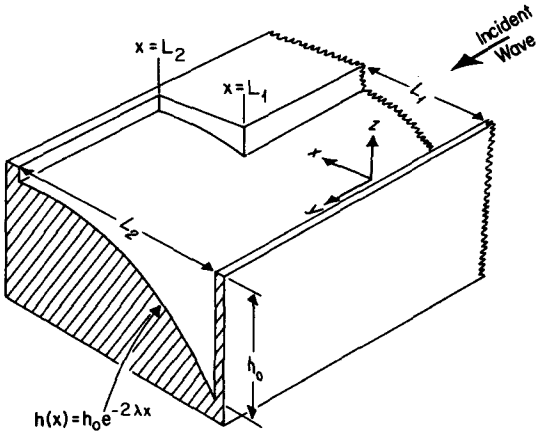

FIG. 2. Problem geometry.

has no signal in the streamfunction. Despite this vanishing velocity, the degenerate Kelvin mode is still capable of propagating energy in a semi-infinite ocean because it no longer decays offshore. However, in the present analysis, the flow is confined to a coastal channel of finite width so the vanishing alongshelf velocity leads to vanishing energy flux. Thus, a nonzero value of C, while indicating that a Kelvin wave is generated, is not associated with any propagation of energy. Equations (14) and (18) may be substituted into (17) to obtain

$$\sum_{q=1}^{\infty} B_q \phi_{2q} = \begin{cases} \hat{A}\phi_{1I} + \sum_{p=1}^{\infty} A_p \phi_{1p}, & 0 < x < L_1 \\ 0, & L_1 < x < L_2 \end{cases} \tag{19a}$$

and

$$\sum_{q=1}^{\infty} B_q \frac{\omega}{l_{2q}} \frac{d\phi_{2q}}{dx} + \frac{h}{h_0} fC = \hat{A}\frac{\omega}{\bar{l}} \frac{d\phi_{1I}}{dx} + \sum_{p=1}^{\infty} A_p \frac{\omega}{l_{1p}} \frac{d\phi_{1p}}{dx}, \quad 0 < x < L_1 \tag{19b}$$

The orthogonality property (12) is applied as in Yeh (1975) in the evaluation of

$$\int_0^{L_2} (19a)\, e^{2\lambda x} \phi_{2n} dx \tag{20a}$$

$$\int_0^{L_1} (19b)\, e^{2\lambda x} \phi_{1m} dx \tag{20b}$$

to obtain a set of linear equations for the A_p

$$E_m C + \frac{1}{fL_2} \sum_{p=1}^{\infty} \left\{ \frac{-\omega}{l_{1p}} H_{mp} + \sum_{q=1}^{\infty} \frac{\omega}{l_{2q}} J_{qp} K_{mq} \right\} A_p = \hat{A} \frac{\omega}{fL_2} \left(\frac{\omega}{\bar{l}} H_{mI} - \sum_{q=1}^{\infty} \frac{\omega}{l_{2q}} J_{qI} K_{mq} \right) \quad m = 1, 2, 3 \cdots \tag{21}$$

where

$$E_m = \frac{2}{L_2} \int_0^{L_1} \phi_{1m} dx \tag{22}$$

$$H_{mp} = 2 \int_0^{L_1} \frac{d\phi_{1p}}{dx} e^{2\lambda x} \phi_{1m} dx \tag{23}$$

$$J_{np} = \frac{2}{L_2} \int_0^{L_1} \phi_{1p} e^{2\lambda x} \phi_{2n} dx \tag{24}$$

$$K_{mq} = 2 \int_0^{L_1} \frac{d\phi_{2q}}{dx} e^{2\lambda x} \phi_{1m} dx. \tag{25}$$

After solving (21) for the A_p and C, the B_q are obtained directly from

$$B_q = \hat{A} J_{qI} + \sum_{p=1}^{\infty} J_{qp} A_p. \tag{26}$$

A parallel analysis for the case $L_1 > L_2$ leads to a similar solution.

$$\frac{L_1}{L_2} E_m^* C + \frac{1}{fL_2} \sum_{q=1}^{\infty} \left\{ \frac{\omega}{l_{2q}} H_{mq}^* - \sum_{p=1}^{\infty} \frac{\omega}{l_{1p}} K_{mp}^* J_{pq}^* \right\} B_q = \hat{A} \frac{1}{fL_2} K_{mI}^* \left(\frac{\omega}{\bar{l}} - \frac{\omega}{l_{1I}} \right) \tag{27}$$

$$A_p = -\hat{A}\delta_{Ip} + \sum_{q=1}^{\infty} J_{pq}^* B_q \tag{28}$$

where E^*, H^*, J^* and K^* are equivalent to the integrals E, H, J and K defined above but with L_1 replacing every occurrence of L_2 and vice versa.

To obtain a solution, the infinite set of equations (21) is truncated at $M + 1$. Then the constant C and the amplitudes A_p are computed for the first M modes. The results presented in the following section were obtained by selecting $M = 40$ and by truncating the inner summation over q at 60 modes. This was sufficient to determine the amplitudes of the lowest 5 modes to within 1 percent (and the lowest 15 modes to within 5 percent) of the solution obtained by using $M = 100$ modes and an inner summation over q of 200 modes.

To verify the accuracy of the solutions, a check on energy conservation was made. The alongshelf energy flux in the wave field is given by the time-averaged product of pressure and alongshelf transport integrated across the shelf:

$$\mathbf{F} = \int_0^L \overline{(g\eta) \cdot (hv)} dx. \tag{29}$$

The overbar denotes a time average. Huthnance (1975) showed that if a set of shelf waves have ω specified, the wave energy flux separates into contributions from individual modes with no contribution from interactions between modes. Evaluation of (29) for a single mode gives

$$\mathbf{F}_n = \frac{1}{4} \frac{|A_n|^2 f\lambda L}{h_0} \left(1 - \frac{\omega l}{f\lambda} \right) \tag{30}$$

where A_n is the wave amplitude. The total radiated energy flux is obtained by summing this quantity over all propagating modes. In all cases, the sum of the reflected and transmitted energy fluxes was within 0.01 percent of the incident energy flux.

It is also of interest to examine the form of the solution under the long-wave and accompanying low-frequency assumptions. While it might be expected that the abruptness of the coastline change would render the long-wave approximation invalid, a well-behaved solution is obtainable for the case $L_2 > L_1$. For long waves, the dispersion relation (11) simplifies to $\omega = 2\lambda f l_n/(k_n^2 + \lambda^2)$ which admits only a single class of waves, all of which propagate and have group velocity in the same direction as phase speed. There are, therefore, no waves available to carry a reflected flux of energy so the coefficients A_p in (14) and (18) vanish. Applying the matching conditions (17) and using the orthogonality relation as in (19) gives the simple solution

$$B_q = \hat{A} J_{qI} \quad q = 1, 2, 3 \cdots \tag{31a}$$

$$E_m C = \frac{1}{fL_2}\left(\hat{A}\hat{c} H_{mI} - \sum_{q=1}^{\infty} B_q c_{2q} K_{mq}\right)$$

$$m = \text{any integer} \tag{31b}$$

where $\hat{c}$ and c_{2q} are the nondispersive long-wave phase speeds (ω/l) of the incident and scattered waves, respectively.

For the case $L_1 > L_2$, the boundary condition $\psi = 0$ along $y = 0$, $L_2 < x < L_1$ cannot be satisfied and the long-wave limit fails.

3. Results

The features of the solution may be illustrated by investigating the effect of varying the five free parameters of the model. These are: ω/f, the incident wave frequency relative to the inertial frequency; I, the incident wave mode number; and the three length scales λ, L_1 and L_2. The length scales form three dimensionless groups: L_2/L_1, λL_1 and λL_2. L_2/L_1 is the relative change in shelf width encountered by the wave while λL_1 and λL_2 represent the respective nondimensional slope steepnesses. Inspection of (21) and (26) shows that the solution is unaffected by the deep ocean depth h_0.

a. Relative shelf width L_2/L_1 varies

The partitioning of the total scattered energy flux into individual transmitted and reflected modes is shown in Fig. 3a for a mode 1 incident wave with $\omega/f = 0.1$ and L_2/L_1 in the range 0.5 to 2.25. The slope steepness over $y < 0$ is fixed at $\lambda L_1 = 1$ so that the incident wave form does not vary. For $L_2/L_1 < 0.8$ an appreciable amount of energy (>5 percent) is reflected. As noted previously, the present barotropic solution is likely to be qualitatively in error in this range, so discussion of narrowing shelf ($L_2/L_1 < 1$) results will be henceforth omitted. For a widening shelf, energy is readily transferred into higher modes. For example, at $L_2/L_1 = 1.5$, transmitted mode 2 carries 33 percent of the scattered energy. Energy may also be transferred to modes lower than the incident. For example, Fig. 3b shows the same situation as in Fig. 3a but with a mode 2 incident wave. At $L_2/L_1 = 1.5$, 7 percent of the incident energy has been transferred to transmitted mode 1 despite the cross-shelf structure being very different from that of the incident wave. In general, the mode most readily excited is that which best fits the cross-shelf structure of the incident wave. A given transmitted mode q has a cross-shelf structure of the form $\sin q\pi x/L_2$ which is similar to that of the incident wave, $\sin I\pi x/L_1$, in the vicinity of $q/L_2 = I/L_1$. It may be expected then that each mode q attains its maximum amplitude near $L_2/L_1 = q/I$. This is verified in Fig. 4 where the transmitted mode amplitudes for the cases in Fig. 3 are plotted. At the local maxima, the amplitudes of the other modes do not vanish since a single transmitted mode is not sufficient to satisfy the condition $\psi = 0$ along the solid wall at $y = 0$. A significant contribution of the other modes is still required.

b. Frequency ω/f varies

In this case the shelf geometry and incident mode number are fixed ($L_2/L_1 = 2.25$; $\lambda L_1 = 1.0$; $I = 1$) while the wave frequency is varied. At low frequency, the modal partitioning of energy flux (Fig. 5a) and the scattered mode amplitudes (Fig. 5b) become independent of ω/f. Their values are asymptotic to the results obtained from (31) indicating that the long-wave limit

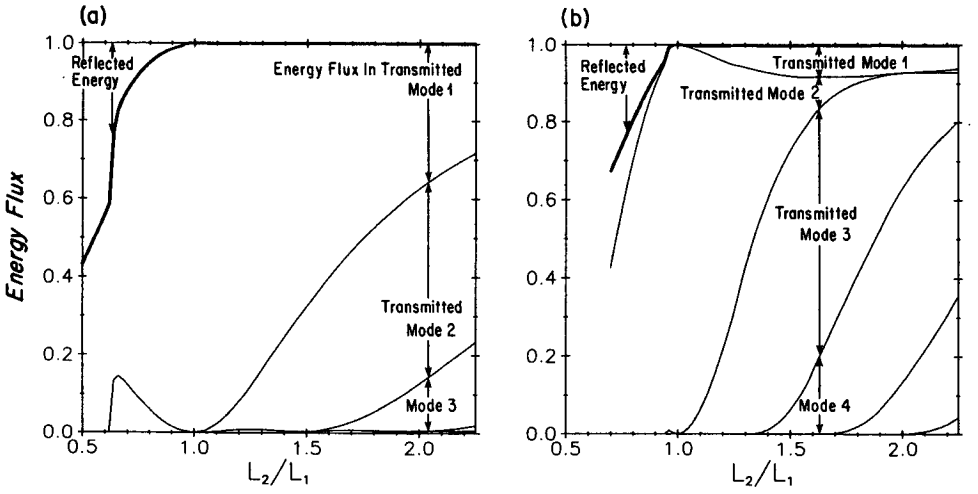

FIG. 3. Modal energy fluxes normalized by the incident wave energy for $\omega/f = 0.1$, $\lambda L_1 = 1.0$, and L_2/L_1 in the range 0.5 to 2.25. The heavy line is the total transmitted energy. The light lines divide the energy between the various modes. (a) Mode 1 incident. (b) Mode 2 incident.

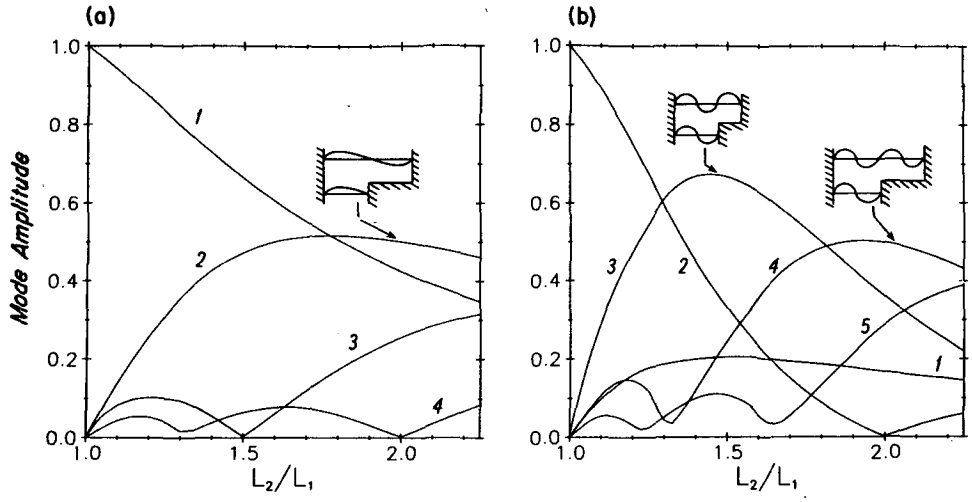

FIG. 4. Magnitudes of transmitted mode amplitudes for the parameter range considered in Fig. 3. Each mode q attains its maximum amplitude near $L_2/L_1 = q/I$ (where I is the incident mode number) since this is where its cross-shelf structure most closely coincides with that of the incident wave.

appears valid despite the abruptness of the coastline variation.

As ω/f increases, the higher modes reach their cutoff frequencies and cease to propagate energy. In this example, for $\omega/f > 0.232$ only two transmitted modes propagate. The energy carried by transmitted mode 3 diminishes rapidly as the cutoff frequency is approached and the group speed tends to zero. In passing through the cutoff frequency, the real part of the wavenumber does not change appreciably while the imaginary part increases slightly from zero. Thus the transition is not strongly manifested in the matching conditions, so the amplitudes of the remaining propagating transmitted modes do not alter significantly. This may be seen by examining the mode amplitudes plotted in Fig. 5b. The energy flux carried in each of the remaining modes does not alter appreciably either, but the significant level of energy previously carried in mode 3 must be directed somewhere. It appears in the excitation of the lowest mode reflected wave. This shows that even for a widening shelf, the barotropic model predicts backscattering of shelf waves at high frequency. Therefore, the application of the model results should be restricted to cases in which the higher transmitted propagating modes carry minimal amounts of energy so that reflected waves will not be generated as the cutoff frequencies of those modes are approached.

c. *Slope steepness λL varies*

The relative shelf width is held constant at $L_2/L_1 = 2.25$, a value which produced strong coupling between modes in the preceding results, and the slope steepnesses are varied. The energy flux partitioning is shown in Fig. 6 for both mode 1 and mode 2 incident waves for $\omega/f = 0.1$ as λL_2 is varied from 1.125 to 4.0. Correspondingly, λL_1 varies from 0.5 to 1.78. For small values of λL_2, where the energy partitioning fluctuates, either the slope steepness or shelf width is small. On such a shelf, inspection of Fig. 1 shows that few modes are available to propagate energy. In the mode 2 incident case, it is seen that some reflection of energy occurs in the range $\lambda L_2 < 1.58$. As λL_2 decreases through the value 1.58, mode 5 ceases to propagate so that, by the same mechanism already described for increasing ω/f, the significant energy flux previously carried by this mode is directed into the reflected modes. This suggests that the model results may not be applicable to narrow or weakly sloping shelves. For moderate to larger values of λL_2, the mode coupling is only weakly dependent on slope steepness; this suggests that the results presented here would change little if a depth profile more general than the exponential were used.

d. *Trapped field*

Over the entire parameter range considered in Fig. 3 ($1 < L_2/L_1 < 2.25$; $\lambda L_1 = 1.0$; $\omega/f = 0.1$) the amplitudes of the evanescent transmitted modes are an order of magnitude smaller than the principal propagating modes. The trapped field is therefore much weaker than the propagating field. As an example, transmitted wave amplitudes for the case $\omega/f = 0.1$, $L_2/L_1 = 2.25$, $\lambda L_1 = 1.0$ are presented in Table 1. From these values are computed the current ellipses for the total field and the trapped field shown in Fig. 7. The trapped-field current ellipses are plotted with a scale 20 times greater than the total field ellipses which further indicates their lack of contribution to the overall flow. Also given in Table 1 are the e-folding scales of

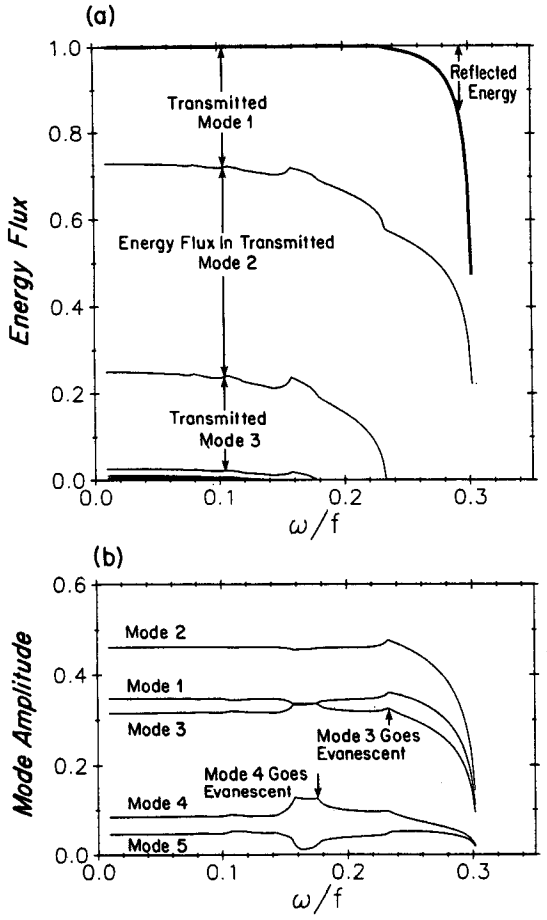

FIG. 5. (a) Modal energy fluxes normalized by incident energy for mode 1 incident, $\lambda L_1 = 1.0$ and $L_2/L_1 = 2.25$ as a function of ω/f. The heavy line is the total transmitted energy. Above the cutoff frequency for mode 3 ($\omega/f = 0.232$) reflection of energy occurs. (b) Corresponding magnitudes of mode amplitudes. As $\omega/f \rightarrow 0$ the scattered wave amplitudes become independent of frequency.

the evanescent modes. Comparison with Fig. 7b shows that the alongshelf extent of the evanescent field is approximately equal to the e-folding scale ($0.2L_1$) of the lowest trapped mode (mode 8). The total field shows the presence of a shadow zone of weak flow downstream ($y > 0$) of the coastline bend and no intensification near the corner. A plot of time and depth averaged kinetic energy (KE) density (Fig. 8) shows that the KE density in the shadow zone is less than 1/20 of that along the upstream coast ($y < 0$). Therefore, both components of the velocity must be very weak in this region, suggesting that the presence of a solid wall along, say, the unit KE density contour in Fig. 8 should produce minimal alteration to the scattered wave solution since the boundary condition of no flow through the wall is already approximately satisfied.

The alongshelf extent of the shadow zone increases linearly with increasing L_2/L_1 and increases approximately as $(\omega/f)^{-1}$. This behavior is expected because of the tendency for low-frequency flow to follow f/h contours (isobaths on an f-plane). As L_2/L_1 increases, the relative change in coastal depth increases, so that the flow requires a longer alongshelf distance to make the adjustment, i.e., a longer shadow zone. Similarly, as the frequency decreases (for fixed L_2/L_1), the flow becomes more geostrophic and must follow the isobaths more closely, resulting in a longer shadow zone. The presence of the shadow zone suggests that shelf width variations which occur over an alongshelf distance comparable to or shorter than the length of the shadow zone should appear sufficiently abrupt to cause significant scattering.

e. Far field

For the case considered in Table 1, the first three transmitted modes have comparable amplitudes but quite different wavelengths. These waves interact to produce a strong alongshelf modulation of the flow pattern downstream from the coastline bend. This can be seen in Fig. 9 which presents an instantaneous contour plot of the surface height displacement. The simple cellular pattern of the crest and trough of the mode 1 incident wave scatters into a complex pattern with strong alongshelf and cross-shelf variability. The importance of the modal interaction is emphasized in Fig. 10 which shows the phase and maximum range of surface height displacement along the coast. The uniform range and linear increase in phase upstream of the bend

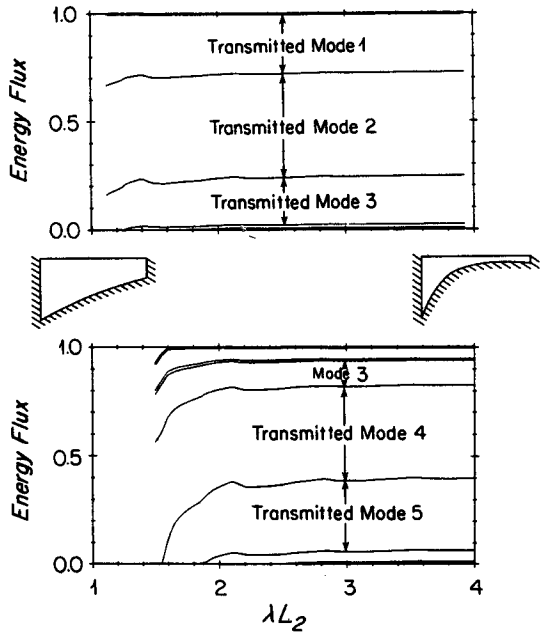

FIG. 6. Normalized modal energy fluxes for $\omega/f = 0.1$, $L_2/L_1 = 2.25$ as a function of λL_2 (and λL_1). Upper panel: Mode 1 incident. Lower panel: Mode 2 incident. The modal partitioning of energy becomes independent of λL at the moderate to high values typical of many continental shelves.

TABLE 1. Properties of the first 11 transmitted modes for the case: mode 1 incident; $\omega/f = 0.1$; $\lambda L_1 = 1.0$; $L_2/L_1 = 2.25$. Amplitudes are normalized by the incident mode amplitude. Characteristic alongshelf scale tabulated is the wavelength for the propagating modes and e-folding distance from $y = 0$ for the evanescent modes. In this case the solution gives a value of $0.197\hat{A}$ for the constant C.

	Propagating modes							Evanescent modes			
Mode number (q)	1	2	3	4	5	6	7	8	9	10	11
Amplitude ($\lvert B_q\rvert/\hat{A}$)	0.346	0.461	0.316	0.085	0.047	0.043	0.013	0.026	0.005	0.013	0.005
Alongshelf scale	(wavelength/L_1)							(e-folding length/L_1)			
	42.3	14.0	6.45	3.56	2.16	1.36	0.77	0.20	0.13	0.10	0.09

attest to the weakness of the backscattered field. Downstream, the varying range suggests that observers comparing sea-level oscillations at different locations along the coast could obtain erroneous estimates of continental shelf wave energy and phase speed if they were not cognizant of the scattering process in effect. Similarly, the cross-shelf structures of surface height variation (shown inset in Fig. 10) exhibit local maxima in sea-level range well offshore, suggesting that weak shelf wave activity observed in coastal sea level could be misleading.

4. Discussion

Before considering the implications of the preceding results for shelf wave scattering in a real coastal ocean, it is instructive to review the limitations of the model from which the results were derived.

Care has been taken in the present analysis to avoid solutions where energy is scattered into barotropic short waves which would be substantially altered and might be altogether absent in a realistically stratified ocean. In general, reflected short waves are not generated when the following conditions apply: (i) The shelf widens ($L_2/L_1 > 1$), (ii) the slope steepness parameters are not too small ($\lambda L_2 \geq 2$) and (iii) wave frequencies are small ($\omega/f \leq 0.2$).

Together, these conditions effectively ensure that there are a large number of propagating modes available to transmit energy forward of the coastline bend, so that energy may be conserved without exciting reflected waves. For a given shelf geometry, stratification increases the frequency at which a wave propagates, so there will be more propagating modes in the stratified case than in the barotropic case. This suggests that the results of the present analysis may be applicable over a broader range of parameters.

Neither the exponential topography nor the abruptness of the coastline bend appear to be limiting assumptions. The scattered wave amplitudes are not strongly dependent on λL for values typical of many

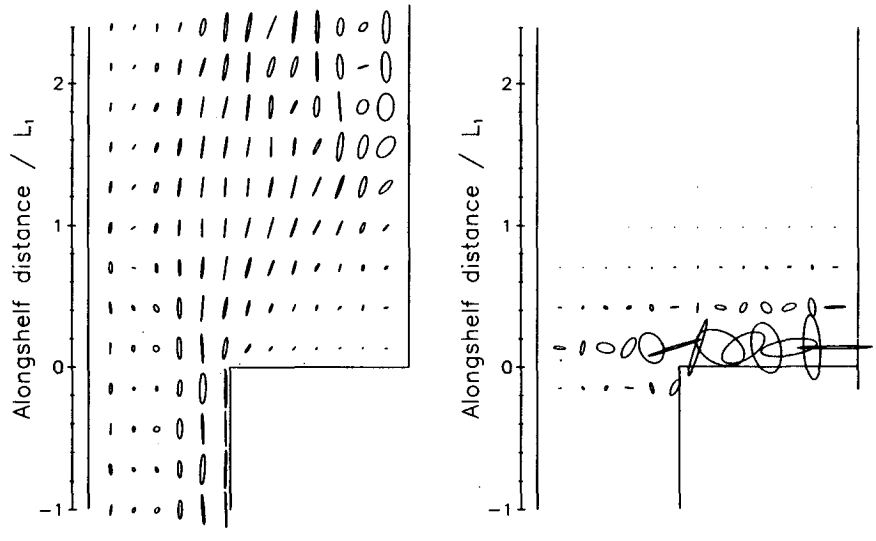

FIG. 7. Current ellipses for $\omega/f = 0.1$, $\lambda L_1 = 1$, $L_2/L_1 = 2.25$. Left: Total field. Right: Evanescent modes only. The velocity scale used to plot the evanescent modes is greater by a factor of 20 than that used for the total field which indicates the weakness of the trapped field relative to the propagating field.

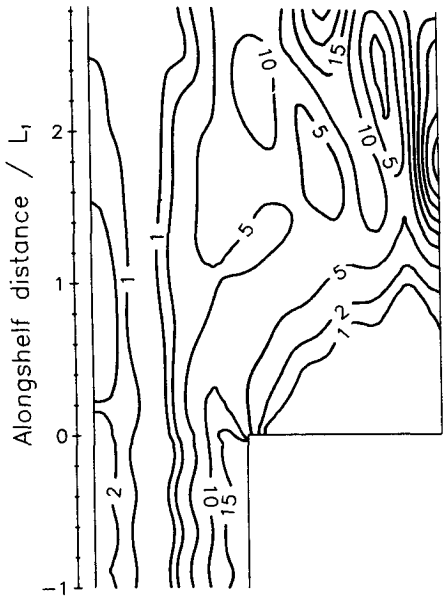

FIG. 8. Time and depth averaged kinetic energy (KE) density for $\omega/f = 0.1$, $\lambda L_1 = 1$, $L_2/L_1 = 2.25$. A shadow zone of weak flow is present behind the coastline bend suggesting that were the, say, unit KE contour to be a solid wall, the solution should differ little.

continental shelves. This indicates that details of the shelf profile do not significantly affect the scattering process. The presence of a shadow zone of very weak currents behind the coastline bend suggests that a more general, less abrupt variation in shelf width, occurring over an alongshelf distance shorter than or comparable to the length of the shadow zone, should still produce the strong mode coupling evident in the present solution.

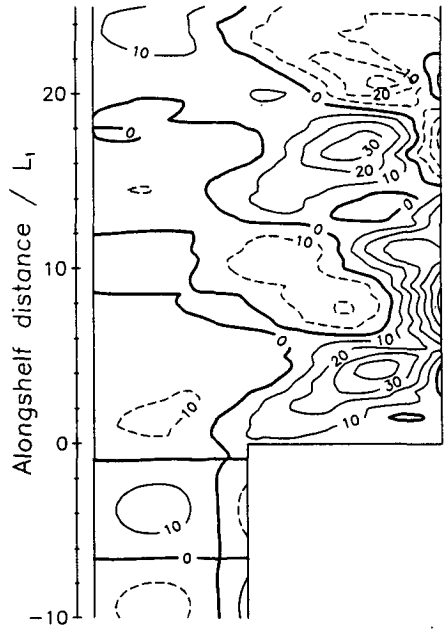

FIG. 9. Instantaneous sea level displacement for $\omega/f = 0.1$, $\lambda L_1 = 1$, $L_2/L_1 = 2.25$. The simple cellular pattern of a mode 1 incident wave is scattered into a complex pattern of interacting modes. The alongshelf scale is compressed.

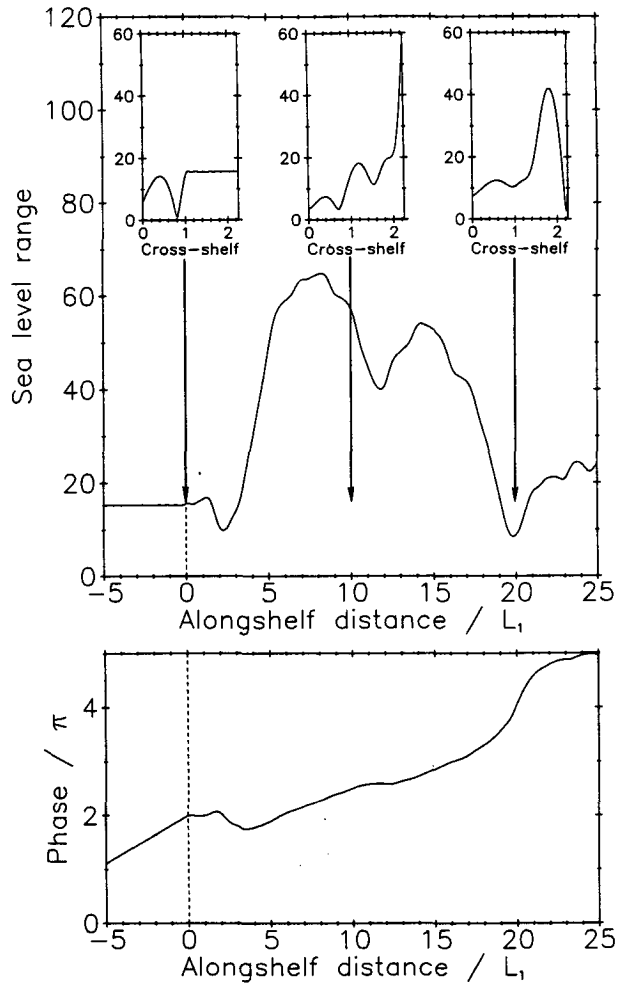

FIG. 10. Range and phase of sea-level fluctuations along the coast (i.e., $x = L_1$, $y < 0$; $x = L_2$, $y > 0$) for $\omega/f = 0.1$, $\lambda L_1 = 1$, $L_2/L_1 = 2.25$. The cross-shelf structure at selected stations (including the coast along $y = 0$, $L_1 < x < L_2$) is shown inset.

The solution to the model equations is assumed to be periodic both in space and time. However, the scattering of a nondispersive shelf wave "pulse" of limited alongshelf extent can be considered by superposing many periodic solutions. At the low-frequency limit, the present solution shows that a continuous wave is scattered into several modes with the partitioning being nearly independent of frequency and wavenumber. Under these conditions, the wavenumber spectra[1] of

[1] The term "spectrum" refers to the complex Fourier transform into wavenumber space of the alongshelf structure of the shelf wave pulse and should not be confused with a power spectrum which contains no phase information.

the scattered wave components will be proportional to the wavenumber spectrum of the incident wave (see Appendix) so that the components of each scattered mode will combine to produce a wave pulse of that mode. Thus, a long shelf-wave pulse will scatter into a train of pulses of differing modes, each traveling at its own free-wave speed and having an amplitude given by the periodic wave solution obtained here. This behavior is exact if the long-wave limit is assumed a priori.

So far, bottom frictional damping has not been included in the model. One might expect that frictional effects would eliminate the need to identify high mode waves in shelf wave observations because the higher mode waves would be damped over a length scale much shorter than that of the lowest mode. To demonstrate that this is not the case, the analysis of Brink and Allen (1978) can be applied to the present model. The effect of weak bottom friction at lowest order is to damp barotropic free waves exponentially over a length scale $\Delta_q = (E^{1/2}a_{qq})^{-1}$. Here, $E^{1/2}$ is an Ekman number defined by

$$E^{1/2} = \left(\frac{1}{2}A_v \Big/ f\right)^{1/2} \Big/ h_0$$

where A_v is a constant vertical eddy viscosity and

$$a_{qq} = \frac{1}{\lambda L}\int_0^L \frac{h_0^2}{h^2}\frac{d\phi_q}{dx}\frac{d\phi_q}{dx}\,dx.$$

Using this result, the effect of friction may be introduced into the present solution by exponentially damping each transmitted mode from its initial value at $y = 0$. Frictional coupling between modes enters at second order. The above definitions differ slightly from Brink and Allen's because, in the present notation, h_0 is the depth at the offshore boundary rather than the depth at the coast. Consequently, the Ekman number used by Brink and Allen (1978, 1983) in their calculations ($E_0^{1/2} = 0.06$) must be multiplied by the relative depth change across the shelf to get $E^{1/2}$. For the example parameters used in Table 1, this gives $E^{1/2} = 6.7 \times 10^{-4}$, and the corresponding values of Δ_q for the first three modes are: $\Delta_1 = 14.7L_2$, $\Delta_2 = 5.96L_2$ and $\Delta_3 = 3.16L_2$. With friction included, the alongshelf modulation of coastal surface height range (Fig. 11) due to interacting modes is less pronounced than in the frictionless case (Fig. 10), but it may still be important observationally.

Periodic wind forcing along a coast is expected to radiate free waves of all modes at the forcing frequency (Gill and Schumann, 1974). The lowest modes are generally the most readily excited, suggesting that the energy propagating in mode 1 should dominate that of higher modes. Scattering can act to reverse this situation. For example, consider two waves of the same frequency simultaneously incident upon a coastline discontinuity, such as might be generated by distant wind forcing. Table 2 shows two different superpositions of the scattered waves resulting from an incident

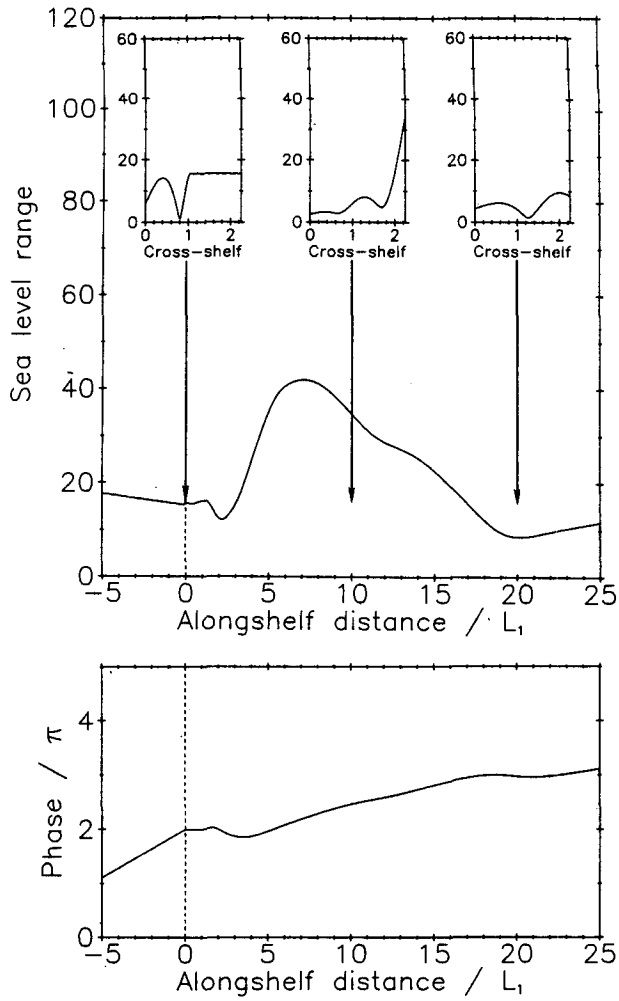

FIG. 11. As in Fig. 10 but with weak bottom friction included.

second mode wave having half the amplitude of the incident first mode wave. The magnitude of mode 3 relative to mode 1 changes markedly depending on whether the incident waves are in phase ($\hat{A}_2 = \frac{1}{2}$) or 180° out of phase ($\hat{A}_2 = -\frac{1}{2}$) at $y = 0$. Such a shift in relative phase of the incident waves could occur if the generating weather system were to be displaced up or down the coast. This simple idea, in which the apparent scattering ability of a particular shelf geometry depends on the incident wave pattern, is suggestive of the confounding role that scattering can play in the interpretation of shelf wave observations.

Some qualitative features of the present solution have apparently been observed recently by Griffin and Middleton (1986) off the east coast of Australia at the southern end of the Great Barrier Reef. There, the promontory of Fraser Island causes a sudden increase in shelf width to the north. Over the wider shelf, Griffin and Middleton fit observed alongshelf velocities to a sum of free CTW modes. Near the coast the modes added in near antiphase to produce currents much

TABLE 2. Superposition of scattered modes from two incident waves of frequency $\omega/f = 0.1$. The geometry is $\lambda L_1 = 1.0$, $\lambda L_2 = 2.25$, $L_2/L_1 = 2.25$. Energy fluxes are normalized by the incident energy.

Mode q	Transmitted Mode Amplitudes (First subscript denotes incident mode number)		Incident Waves in phase at $y = 0$		Incident Waves 180° out of phase at $y = 0$	
	B_{1q}	B_{2q}	$\lvert B_{1q}+1/2B_{2q}\rvert$	Energy flux	$\lvert B_{1q}-1/2B_{2q}\rvert$	Energy flux
1	$0.346 + i0.001$	$-0.145 - i0.003$	0.274	0.146	0.419	0.342
2	$0.461 + i0.001$	$-0.059 - i0.002$	0.431	0.351	0.490	0.455
3	$0.316 - i0.001$	$0.219 + i0.002$	0.425	0.323	0.206	0.076

weaker than those observed further offshore. Closer to Fraser Island they added even closer to antiphase, which is suggestive of a CTW shadow zone behind Fraser Island. The occurrence of a shadow zone and the indication that significant levels of energy are present in multiple modes are both consistent with scattering due to the changing shelf width. Furthermore, Griffin and Middleton conclude that the current variability north of Fraser Island results from CTWs which propagate into the study region from somewhere south of Fraser Island.

Finally, the model presented here represents only an initial step toward understanding the importance of shelf wave scattering in coastal processes. Further studies are needed which generalize the present results to more realistic geometries, and most importantly, which include realistic stratification so that new situations (e.g., a narrowing shelf) can be studied without the limitations of a barotropic model.

5. Summary

A barotropic continental shelf wave of frequency ω traveling along a shelf whose width changes abruptly from L_1 to L_2 at some point scatters into all allowable modes of that frequency. A solution for the scattered wave amplitudes has been obtained for the case of an exponential cross-shelf depth profile, $h(x) = h_0 e^{-2\lambda x}$. Discussion is limited to solutions in which reflected short waves, which might not be present in a realistically stratified ocean, are not generated. This requires that the shelf widens ($L_2/L_1 > 1$), the slope steepness is not too small ($\lambda L \gtrsim 2$), and the wave frequency is low ($\omega/f \lesssim 0.2$). Within this parameter range, the following barotropic results should remain valid for a stratified coastal ocean.

1) The solution is relatively insensitive to the steepness of the exponential profile (λL) which suggests that the results are qualitatively applicable to more general cross-shelf depth profiles.

2) The transmitted mode which is most readily excited is that which has a cross-shelf structure most closely coinciding with that of the incident wave. For a widening shelf, energy is therefore readily transferred to higher modes.

3) For a widening shelf, there is a shadow zone of weak flow behind the coastline bend. The strong mode coupling is therefore primarily a result of the absolute width change and not merely its abruptness.

4) A nondispersive shelf wave "pulse" of limited alongshelf extent scatters into a train of similarly shaped waves of all allowable modes, each propagating at its own free-wave speed.

5) The interaction of the scattered modes strongly modulates the magnitude and phase progression of the flow field downstream of the scattering region. This modulation occurs over an alongshelf distance too short for the effect to be eliminated by weak frictional damping of the higher modes.

6) The scattered waves resulting from multiple incident waves of different modes can interfere to enhance the energy in some modes while reducing that in others.

Acknowledgments. The authors are indebted to Ken Brink and Allan Clarke for their critical reviews of an earlier version of the manuscript. This research was supported by the National Science Foundation under Grant OCE84-17769.

APPENDIX

Scattering of a Shelf Wave Pulse

Consider an incident shelf wave of limited alongshelf extent represented by a superposition of periodic waves with a continuum of wavelengths:

$$\psi_I(x, y, t) = \phi_{1I}(x) \int_{-\infty}^{\infty} A(\hat{l}) e^{i\hat{l}(y-\hat{c}t)} d\hat{l} \qquad \text{(A1)}$$

Provided the amplitude spectrum $A(\hat{l})$ is limited to small wavenumbers, the phase speed $\hat{c} = \omega/\hat{l}$ will be a constant dependent only on the shelf geometry and the "pulse" will maintain a permanent form as it propagates. At the low frequency, small wavenumber limit, it has been demonstrated in section 3 that a single incident continuous wave scatters into a train of transmitted waves of amplitudes B_q with the B_q being functions only of the shelf geometry. For a unit amplitude

incident wave, this scattering process may be summarized as

$$\phi_{1l}(x)e^{i(\hat{l}y-\omega t)} \rightarrow \sum_{q=1}^{\infty} B_q(\lambda, L_1, L_2)\phi_{2q}(x)e^{i(l_{2q}y-\omega t)} \quad \text{(A2)}$$

Since the scattering model is linear, it follows that the pulse will scatter as

$$\psi_I(x, y, t) \rightarrow \int_{-\infty}^{\infty} \sum_{q=1}^{\infty} A(\hat{l})B_q(\lambda, L_1, L_2)\phi_{2q}(x)e^{i(l_{2q}y-\omega t)}\, d\hat{l}.$$

Noting that $\omega = \hat{c}\hat{l} = c_{2q}l_{2q}$, this simplifies to

$$\psi_I(x, y, t) \rightarrow \sum_{q=1}^{\infty} B_q\phi_{2q} \int_{-\infty}^{\infty} A(\hat{l})e^{i(\hat{c}/c_{2q})\hat{l}(y-c_{2q}t)}d\hat{l}. \quad \text{(A3)}$$

Comparison with (A1) shows that the wave components combine to produce a train of pulses of differing modes, each with shape similar to that of the incident wave but stretched in the alongshelf direction of a factor $c_{2q}/\hat{c}$. Each pulse travels at its own nondispersive free wave speed c_{2q}.

REFERENCES

Allen, J. S., 1976: Continental shelf waves and alongshore variations in bottom topography and coastline. *J. Phys. Oceanogr.*, **6**, 864–878.

Battisti, D. S., and B. M. Hickey, 1984: Application of remote wind-forced coastal trapped wave theory to the Oregon and Washington coasts. *J. Phys. Oceanogr.*, **14**, 887–903.

Brink, K. H., 1980: Propagation of barotropic continental shelf waves over irregular bottom topography. *J. Phys. Oceanogr.*, **10**, 765–778.

——, 1982a: The effect of bottom friction on low-frequency coastal trapped waves. *J. Phys. Oceanogr.*, **12**, 127–133.

——, 1982b: A comparison of long coastal trapped wave theory with observations off Peru. *J. Phys. Oceanogr.*, **12**, 897–913.

——, 1986: Scattering of long coastal-trapped waves due to bottom irregularities. *Dyn. Atmos. Oceans*, **10**, 149–164.

——, and J. S. Allen, 1978: On the effect of bottom friction on barotropic motion over the continental shelf. *J. Phys. Oceanogr.*, **8**, 919–922.

——, and J. S. Allen, 1983: Reply (to T. J. Simons' comments on K. H. Brink and J. S. Allen, *J. Phys. Oceanogr.*, **8**, 919–922, 1978). *J. Phys. Oceanogr.*, **13**(1), 149–150.

Buchwald, V. T., 1977: Diffraction of shelf waves by an irregular coastline. *Waves on Water of Variable Depth*, D. G. Provis and R. Radok, Eds., Lecture Notes in Physics, Vol. 64, Springer and Australian Academy of Sciences, 235 pp.

Chao, S.-Y., L. J. Pietrafesa and G. S. Janowitz, 1979: The scattering of continental shelf waves by an isolated topographic irregularity. *J. Phys. Oceanogr.*, **9**, 687–695.

Chapman, D. C., 1983: On the influence of stratification and continental shelf and slope topography on the dispersion of subinertial coastally trapped waves. *J. Phys. Oceanogr.*, **13**(9), 1641–1652.

Clarke, A. J., 1977: Observational and numerical evidence for wind-forced coastal trapped long waves. *J. Phys. Oceanogr.*, **7**, 231–247.

——, and S. Van Gorder, 1986: A method for estimating wind driven frictional, time-dependent, stratified shelf and slope water flow. *J. Phys. Oceanogr.*, **16**, 1013–1028.

Enfield, D. B., and J. S. Allen, 1983: The generation and propagation of sea level variability along the Pacific coast of Mexico. *J. Phys. Oceanogr.*, **13**, 1012–1033.

Gill, A. E., and E. H. Schumann, 1974: The generation of long shelf waves by the wind. *J. Phys. Oceanogr.*, **4**, 83–90.

Griffin, D. A., and J. H. Middleton, 1986: Coastal trapped waves behind a large continental shelf island, southern Great Barrier Reef. *J. Phys. Oceanogr.*, **16**, 1651–1664.

Grimshaw, R., 1977: The effects of a variable Coriolis parameter, coastline curvature and variable bottom topography on continental shelf waves. *J. Phys. Oceanogr.*, **7**, 547–554.

Halliwell, G. R., and J. S. Allen, 1984: Large-scale sea level response to atmospheric forcing along the west coast of North America, Summer 1973. *J. Phys. Oceanogr.*, **14**, 864–886.

Huthnance, J. M., 1975: On trapped waves over a continental shelf. *J. Fluid Mech.*, **69**, 689–704.

——, 1978: On coastal trapped waves: Analysis and numerical calculation by inverse iteration. *J. Phys. Oceanogr.*, **8**, 74–92.

Smith, R. L., 1978: Poleward propagating perturbations in currents and sea levels along the Peru coast. *J. Geophys. Res.*, **83**, 6083–6092.

Yeh, H.-C., 1975: Method of solving potential field problems with complicated geometries. *J. Appl. Phys.*, **46**, 4431–4440.